The Astronomical Journal, 159:203 (9pp), 2020 May https://doi.org/10.3847/1538-3881/ab7d34

High-resolution Optical Spectroscopic Observations of Comet 21P/Giacobini–Zinner in Its 2018 Apparition

Yoshiharu Shinnaka[1], Hideyo Kawakita[1,2], and Akito Tajitsu[3]
[1] Laboratory of Infrared High-resolution Spectroscopy (LiH), Koyama Astronomical Observatory, Kyoto Sangyo University, Motoyama, Kamigamo, Kita-ku, Kyoto 603-8555, Japan; yoshiharu.shinnaka@cc.kyoto-su.ac.jp
[2] Department of Physics, Faculty of Science, Kyoto Sangyo University, Motoyama, Kamigamo, Kita-ku, Kyoto 603-8555, Japan
[3] Subaru Telescope, National Astronomical Observatory of Japan, 650 North A'ohoku Place, Hilo, HI 96720, USA
Received 2019 September 9; revised 2020 March 2; accepted 2020 March 4; published 2020 April 13

Abstract

Comet 21P/Giacobini–Zinner is a peculiar comet from the viewpoints of the chemical and physical properties of its dust grains. We conduct optical high-resolution spectroscopic observations of the comet. The intensity ratios of forbidden oxygen lines (at 557.7, 630.0, and 636.4 nm) and ortho-to-para abundance ratios (OPRs) of water cations (H_2O^+) and amidogen radicals (NH_2) are obtained while only the upper limit for $^{14}N/^{15}N$ in the amidogen radical is restricted. The OPRs of H_2O^+ and NH_2 are similar to those of other comets, although the real meaning of these OPRs is still debated. Based on the observation of the forbidden emission lines of oxygen atoms, it can be concluded that the comet is depleted in CO_2. In consideration with the depletion in other highly volatile species found in the near-infrared region and the presence of complex organics in comet 21P/Giacobini–Zinner, this comet might form in a warmer region in the solar nebula compared with other comets.

Unified Astronomy Thesaurus concepts: Comets (280); Short period comets (1452); Spectroscopy (1558); Comet volatiles (2162)

1. Introduction

Comet 21P/Giacobini–Zinner (hereinafter, 21P/GZ) is classified as a Jupiter-family comet based on its Tisserand parameter with respect to Jupiter ($T_J = 2.46$). According to the previous reports of the observations of comet 21P/GZ, this comet showed unique properties of not only volatiles but also dust grains compared with other comets: (1) depletion of carbon-chain molecules like C_2 and C_3 as well as NH_2 (Fink 2009), (2) depletion of highly volatile species (C_2H_6, CH_3OH, and CO; DiSanti et al. 2013; Dello Russo et al. 2016), and (3) negative linear polarization gradients for reflected sunlight by cometary grains, indicative of existence of organic matter (Kiselev et al. 2000).

Comet 21P/GZ is also known as the parent comet of the October Draconids meteor shower (historically called the Giacobinids), based on the similarity in orbital elements between comet 21P/GZ and the meteoroids of the Giacobinids (Jenniskens 2006). The meteoroids are thought to be porous grain conglomerates. Their derived densities are smaller compared with other meteor showers (0.1–0.5 g cm^{-3}), and they have typical chondritic abundance ratios of the major heavy elements (namely Mg, Fe, and Na), and the Giacobinids meteors exhibit fragmentation behaviors (Borovička et al. 2010, 2014) not frequently seen in other meteor showers.

In summary, from the observational viewpoints, comet 21P/GZ is peculiar among observed comets. The unique properties of comet 21P/GZ might be explained by the different birth place of the comet (formed under different physical conditions such as temperature, dust-to-gas ratio, and ionization degree). Therefore, to understand the physical conditions where icy/dust materials in comet 21P/GZ formed, we conducted optical high-resolution spectroscopic observations of the comet in its 2018 apparition. We tried to determine those properties of volatiles considered as primordial. We report the results of our observations and discuss the origin of comet 21P/GZ.

2. Observations and Data Reduction

High-resolution optical spectroscopic observations of comet 21P/GZ were performed on UT 2018 September 5, 9, and October 3 using the High Dispersion Spectrograph (HDS; Noguchi et al. 2002) attached to the Subaru Telescope in Maunakea, Hawaii. The heliocentric and geocentric distances of the comet were 1.01–1.07 au and 0.39–0.47 au, respectively. The optical peak of the coma was centered on the slit. The spectra covered the wavelength region between 551.4 and 827.9 nm with a gap between 684.5 and 693.4 nm. The slit size was $0\farcs5 \times 8\farcs5$ in the sky. The spectral resolution, $R \equiv \lambda/\Delta\lambda$, was 72,000 over the entire wavelength region. Details of our observations are listed in Table 1. Data taken with the Subaru/HDS were reduced using the IRAF software (distributed by NOAO[4]) using common reduction procedures of the HDS.[5] We extracted one-dimensional spectra of the comet from the spectral images within the aperture of $0\farcs5 \times 7\farcs5$ to avoid the slit-edge regions. The wavelength calibration was performed using the Th–Ar lamp spectrum and finally, the spectra of comet 21P/GZ are represented in the comet's rest frame. The flux calibration was performed using bright early-type stars near the comet during the observation (see Table 1), taking telluric extinction into consideration. The reference stars (and their spectral types) are HD 27026 (B9V) and HD 41161 (O8V) for the observations on UT 2018 September 5 and 9, and are HD 49643 (B8V) and HR 1544 (A1V) on UT 2018 October 3. We assumed the spectrum of each reference star as a blackbody spectrum at a given temperature (effective temperatures of the star).

We subtracted the modeled continuum components (represented as the sunlight reflected by cometary dust grains) from the reduced spectra to extract the emission spectra of the comet.

[4] IRAF is distributed by the National Optical Astronomy Observatory, which (AURA) under cooperative agreement with the National Science Foundation.
[5] http://www.naoj.org/Observing/Instruments/HDS/hdsql-e.html

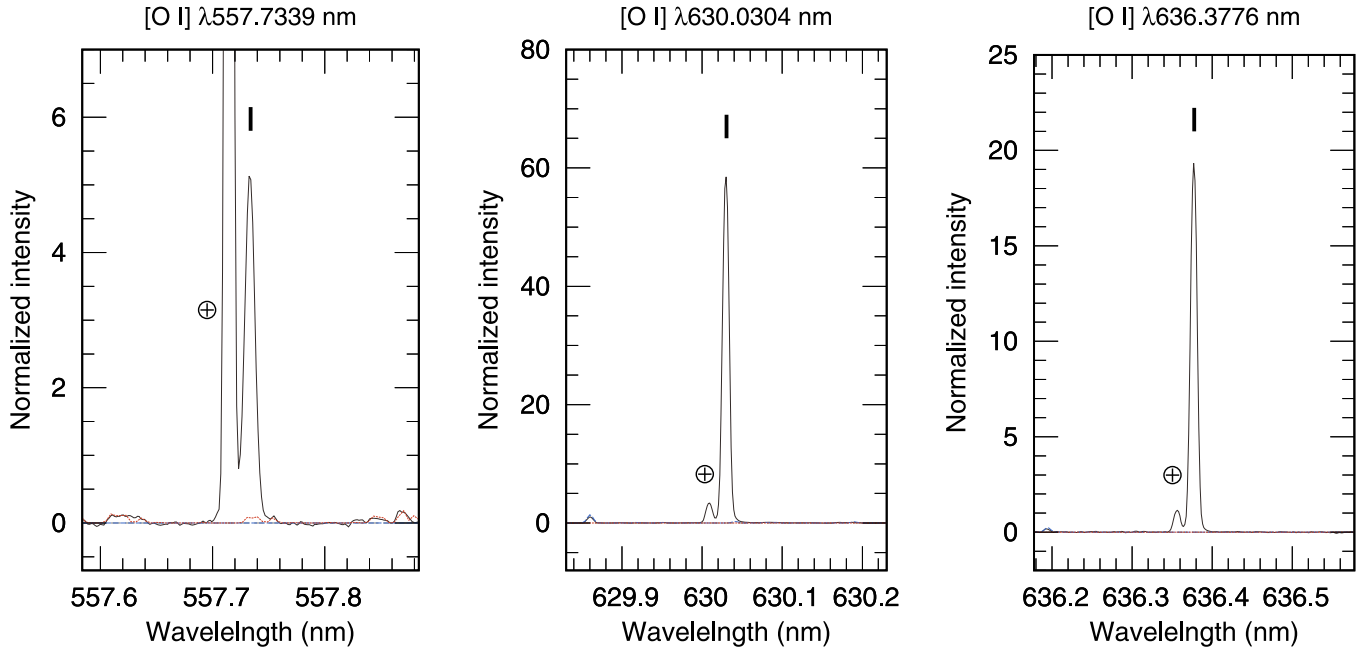

Figure 1. Three [O I] lines in comet 21P/GZ on UT 2018 October 3. The wavelengths are in the cometary rest frame. Vertical tics indicate the [O I] lines of 21P/GZ, and the astrological symbols of Earth (circled "+" marks) located at the shorter wavelength side of each line originated from telluric oxygen. The wavelengths of these telluric [O I] lines were shifted by the relative velocity of the comet to Earth at the observations ($\dot{\Delta} = 10.49$ km s^{-1}). The telluric oxygen emission lines are clearly separated from the cometary lines. We removed the contamination of [O I] emission lines at 557.7 nm by the C_2 (1–2) Swan band system (red line). The contamination by C_2 emission lines with the emission line at 557.7 nm is estimated to be 1.7% ± 0.3%. We can ignore the contamination of [O I] emission lines at 630.0 and 636.4 nm by the NH_2 (0, 8, 0) band (blue line).

Table 1
Observational Circumstances

UT Time in 2018		T_{exp} (s)	r_H (au)	Δ (au)	$\dot{\Delta}$ (km s^{-1})	Airmass	Reference Stars (Airmass)
Sep 5	11:27	12,300	1.015	0.396	−2.93	2.65–1.18	HD 27026 (1.21), HD 41161 (2.39)
Sep 9	12:38	9600	1.013	0.392	−0.48	1.74–1.14	HD 27026 (1.08), HD 41161 (2.13)
Oct 3	13:35	6200	1.066	0.469	10.49	1.43–1.18	HD 49643 (3.37), HR 1544 (1.42)

Note. The first column indicates the start time of the exposures for comet 21P/GZ. T_{exp} is total integration time in seconds. r_H and Δ are heliocentric and geocentric distances at the observations in astronomical units, respectively. $\dot{\Delta}$ is the relative velocity of the comet to Earth at the time of the observations.

The modeled continuum spectrum of the comet is computed as a product of the high-resolution solar spectrum (Kurucz 2005), the reflectance spectrum of the cometary dust grains, and the telluric transmittance spectrum. The reflectance spectrum was obtained by dividing the continuum component of the reduced spectrum by the solar spectrum. The telluric transmittance spectrum was computed using the LBLRTM code (Clough et al. 1992) with weather conditions at the time of the observations. Finally, the modeled continuum spectrum was convolved with the instrumental profile approximated by a Gaussian function corresponding to the spectral resolution.

3. Results and Discussion

3.1. Intensity Ratios of the Three Forbidden Oxygen Lines

In the cometary coma, oxygen atoms are excited to the electronic metastable states of ^{1}S and ^{1}D, and those states emit photons at 557.7 and 630.0/636.4 nm as forbidden lines of oxygen, respectively. Such excited oxygen atoms can be produced via photodissociation of H_2O or other oxygen-bearing molecules like CO_2 in the coma by solar UV radiation. We measured both the intensity and the FWHM of the three [O I] lines by fitting them with a Gaussian profile for the spectrum taken on UT 2018 October 3 (Figure 1). Because the relative velocities between the comet and Earth on UT 2018 September 5 and 9 were too small, the telluric forbidden oxygen emission lines overlapped with cometary lines and could not be separated. The measured line profile of each [O I] emission line in the observed spectrum is a convolution between the intrinsic and instrumental profiles. Therefore, the FWHM of the observed emission line ($FWHM_{obs}$) is expressed by the intrinsic FWHM of the emission line ($FWHM_{intr}$) and the FWHM of the instrumental profile ($FWHM_{inst}$) as

$$FWHM_{obs} = \sqrt{FWHM_{intr}^2 + FWHM_{inst}^2}, \quad (1)$$

where $FWHM_{inst} = 0.00861 \pm 0.00032$ nm is obtained from the telluric nightglow emission lines recorded simultaneously in the spectrum of comet 21P/GZ ([O I] at 557.7, 630.0, and 636.4 nm, and Na I at 589.0 and 589.6 nm).

The [O I] lines at 557.7 nm and 630.0/636.4 nm could be contaminated with the emission lines of the C_2 (1–2) Swan band system and the NH_2 (0, 8, 0) band, respectively. To measure the intensity of these [O I] lines accurately, the contaminations are not negligible and must be removed

Table 2
Results of Three [O I] Emission Lines: Intensity and Intrinsic FWHM of Each Line, Intensity Ratios of Red Doublet and the Green/Red Lines, and Abundance Ratio of CO_2 Relative to H_2O

Intensity [Arbit. Units] (FWHM$_{intr}$ (km s^{-1})[a])			$\frac{I_{630.0}}{I_{636.4}}$	$\frac{I_{557.7}}{I_{630.0}+I_{636.4}}$[b]	$\frac{N_{CO_2}}{N_{H_2O}}$ [%][c]
[O I] λ557.7 nm	[O I] λ630.0 nm	[O I] λ636.4 nm			
0.58 ± 0.01 ($2.05^{+0.16}_{-0.12}$)	5.86 ± 0.06 ($0.90^{+0.22}_{-0.31}$)	1.96 ± 0.02 ($0.99^{+0.20}_{-0.26}$)	2.99 ± 0.04	0.0431 ± 0.0008	(A): 0.9 ± 0.1
…	…	…	…	…	(B): 11.0 ± 0.3

Notes.
[a] FWHM$_{intr}$ (nm) is converted to the most probable velocity for the Maxwell–Boltzmann velocity distribution using Equation (9) in Decock et al. (2013).
[b] Green-to-red line ratio corrected with a collisional quenching factor of 0.58.
[c] CO_2/H_2O abundance ratio is computed from the green-to-red line ratio by Equation (2). The values labeled with (A) and (B) are computed with the parameters of cases (A) and (B) in Table 3, respectively (see the text).

(Decock et al. 2015; Rousselot et al. 2015, and references therein). We measured the emission flux of the [O I] green line at 557.7 nm after removing the contamination by C_2 lines using the C_2 fluorescence excitation model (Shinnaka et al. 2010) with a given vibrational excitation temperature of 4000 K, which is a typical temperature found in comets (Rousselot et al. 2012). The contamination of the emission line at 557.7 nm by C_2 emission lines is estimated to be $1.7\% \pm 0.3\%$. For the [O I] lines at 630.0/636.4 nm, we used the synthetic spectrum of NH_2 based on the fluorescence excitation model of NH_2 (Kawakita et al. 2000) with an ortho-to-para abundance ratio (OPR) of 3.31 (see Section 3.2) to subtract the contamination by NH_2. The contamination of the [O I] lines at 630.0/636.4 nm by NH_2 emission is negligible in our spectrum ($0.3 \pm 0.1\%$ for [O I] at 630.0 nm and no NH_2 emission lines for [O I] at 636.4 nm). Table 2 lists the intrinsic intensity and FWHM of each [O I] line.

The resultant intensity ratio of the [O I] red doublet at 630.0/636.4 nm was 2.99 ± 0.04. The derived green-to-red line ratio of [O I] (the ratio between the intensity of [O I] at 557.7 nm and the total intensity of the [O I] red doublet at 630.0/636.4 nm) was derived to be 0.074 ± 0.001, consistent with H_2O as the dominant source for excited atomic oxygen (Cochran & Cochran 2001). The intrinsic FWHM of the green line is wider than that of the red-doublet lines. These results are listed in Table 2.

The intrinsic FWHM of [O I] at 557.7 nm is wider than those of the [O I] 630.0/636.4 nm lines in contrast with the theoretical prediction for the photodissociation of water (as pointed out by Cochran 2008; Decock et al. 2013). Decock et al. (2013) claimed that CO_2 is photodissociated with more energetic photons than water (that photodissociated mainly by the Lyα photon) and therefore the [O I] emission line at 557.7 nm (expected to be largely contaminated with O(^{1}S) produced from CO_2) should be wider than the [O I] emission lines at 630.0/636.4 nm (those are mainly caused from water and less influenced by CO_2). However, to discuss the kinetic energies (i.e., velocities) of oxygen atoms produced from water and CO_2 by photodissociation, we must consider the photodissociatoin kinematics of the molecules (e.g., Song et al. 2014). An alternative explanation might be possible from the viewpoint of lifetimes of excited oxygen atoms since the lifetimes of excited oxygen atoms (O(^{1}S) and O(^{1}D)) are different by a factor of ~100 (0.79 and 116 s for 1 au from the Sun). Therefore, the probability for collision of O(^{1}D) during its lifetime with other molecules (mainly, water) in the coma is larger than O(^{1}S) by a factor of ~100. The metastable oxygen atoms (O(^{1}S) and O(^{1}D)) are chemically active and their collisions with water molecules easily produce two OH radicals, or the collisions of meta-stable oxygen atoms with water, CO_2, or CO molecules cause non-radiative transitions to lower states (Bhardwaj & Raghuram 2012). Because these collisions of O(^{1}S) and O(^{1}D) with other molecules prevent the [O I] emission, only O(^{1}D) with smaller velocity differences from the background coma molecules can emit the [O I] emission lines at 630.0/636.4 nm while the O(^{1}S) atoms with larger velocity differences from the background can emit the [O I] emission at 557.7 nm. This may be the reason why the [O I] emission line at 557.7 nm is wider than the [O I] lines at 630.0/636.4 nm.

The obtained intensity ratio of the [O I] red doublet (630.0/636.4 nm) is consistent with the ratio of theoretical Einstein's A coefficients for the transitions because those transitions have the same upper state but different lower states (Galavis et al. 1997; Storey & Zeippen 2000). The green-to-red line ratio of [O I] in comet 21P/GZ is similar to the values previously reported for other comets (Capria et al. 2010; Decock et al. 2013; McKay et al. 2013, 2015, 2016, and references therein), supporting the hypothesis that water is the dominant origin of excited oxygen atoms generating these three [O I] emission lines in the coma when a comet was located closer than ~2.5 au from the Sun. This hypothesis is based on the comparison between the observed green-to-red line ratios and the ratios of theoretical emission rates of [O I] lines for different sources (water, CO, and CO_2) as claimed by Cochran & Cochran (2001) and Decock et al. (2013). Recent estimates for the [O I] line ratio in the cases of water, CO, and CO_2 as the source of excited oxygen atoms are found in the literature (Raghuram & Bhardwaj 2013; Decock et al. 2015; Cessateur et al. 2016). We note that no experimentally determined cross-sections for the production of O(^{1}S) in the photodissociation of water are available (Bhardwaj & Raghuram 2012) and also note that the yield of O(^{1}D) in the photodissociation of CO_2 is also not reported in the laboratory (Huestis & Slanger 2006).

Abundance ratio of CO_2/H_2O could be derived from the following formula (same as Equation (12) of Decock et al. 2013):

$$\frac{N_{CO_2}}{N_{H_2O}} = \frac{(G/R)\,W^{red}_{H_2O} - \beta^{green} W^{green}_{H_2O}}{\beta^{green} W^{green}_{CO_2} - (G/R)\,W^{red}_{CO_2}}, \quad (2)$$

where N_X denotes the column density of molecule X, G/R is the green-to-red line ratio, W^{green}_X and W^{red}_X denote photodissociation rates of molecule X producing O(^{1}S) (green) and

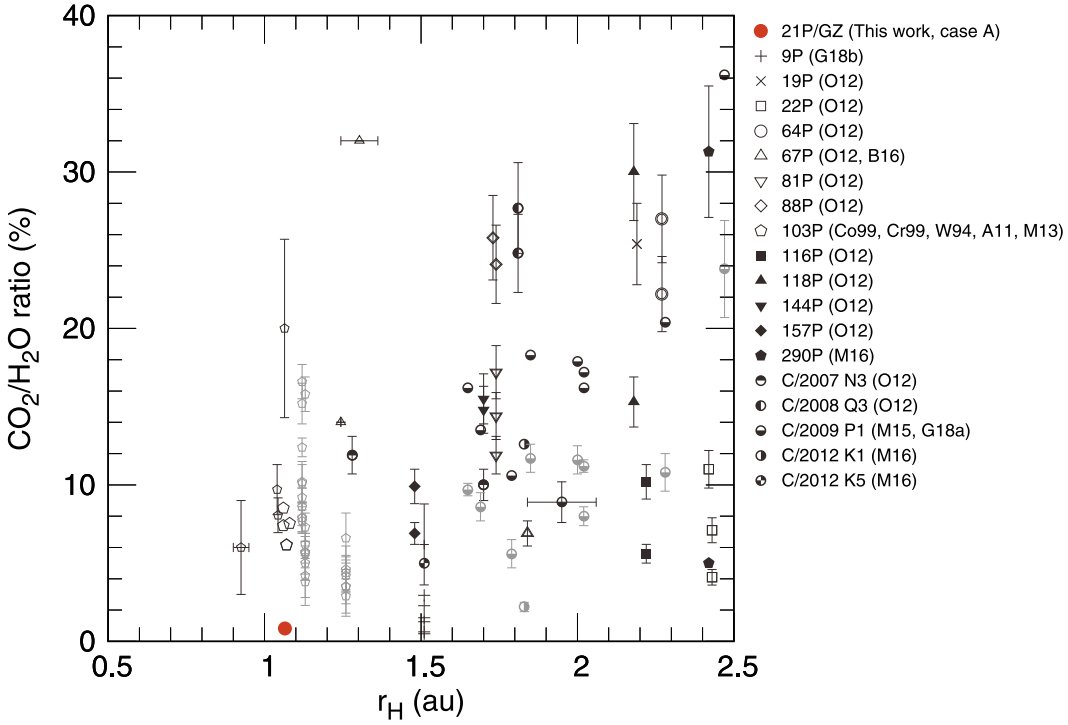

Figure 2. CO_2/H_2O abundance ratios in comets at observed heliocentric distances within 2.5 au. The red (filled circle) symbol is the CO_2/H_2O abundance ratio of 21P/GZ estimated from the green-to-red line ratio of [O I]. The error bar of comet 21P/GZ is smaller than the symbol size. Gray symbols indicate the data in comets estimated from the green-to-red line ratios obtained from ground-based facilities in consideration of the collisional quenching of O(^{1}D) atoms (M13 for McKay et al. 2013, M15 for McKay et al. 2015, and M16 for McKay et al. 2016) and from the CO Cameron-band observations (W94 for Weaver et al. 1994). Black symbols are the CO_2/H_2O abundance ratios in comets estimated from the infrared broadband imaging observations by the Spitzer space telescope (M16 for McKay et al. 2016), and derived from direct measurements of H_2O and CO_2 by the ISO space observatory (Cr99 for Crovisier et al. 1999 and Co99 for Colangeli et al. 1999), the AKARI comet survey program (O12 for Ootsubo et al. 2012), the Deep Impact spacecraft (A11 for A'Hearn et al. 2011, G18a for Gersch et al. 2018a, and G18b for Gersch et al. 2018b), and the Rosetta spacecraft (B16 for Bockelée-Morvan et al. 2016), respectively.

O(^{1}D) (red), and $\beta^{\rm green}$ is the branching ratio of the green line at 557.7 nm for O(^{1}S). Here we assume that only H_2O and CO_2 are the sources of O(^{1}S) and O(^{1}D) atoms in coma. Note that we might have to consider the production of O(^{1}S) and O(^{1}D) by the photodissociation of the O_2 molecule in coma. In fact, the O_2 molecule was detected in comet 67P/Churyumov–Gerasimenko by the Rosetta/ROsetta Spectrometer for Ion and Neutral Analysis (ROSINA) for the first time, and the mean value of the local abundance relative to water was reported as 1.8% ± 0.4% (Altwegg et al. 2019), which is similar to the value found by the re-analysis of in situ data taken in comet 1P/Halley (Rubin et al. 2015). However, based on a recent study by Cessateur et al. (2016), the contributions of O_2 to the production of O(^{1}S) and O(^{1}D) are negligible in comparison with those of water.

We applied two parameter sets, cases (A) and (B) listed in Table 3. The photodissociation rates at 1 au in case (A) are basically based on laboratory studies and taken from Raghuram & Bhardwaj (2013) while those in case (B) are empirical and taken from McKay2015B in Table 6 of McKay et al. (2016). The empirical parameter set successfully reproduced the CO_2/H_2O ratio from the [O I] green-to-red line ratio, consistent with the CO_2/H_2O ratio directly measured in infrared for comet C/2009 P1 (Garradd) and C/2012 K1 (PanSTARRS) although the CO_2/H_2O ratios derived with the parameter set based on laboratory studies are systematically lower than those derived with the empirical parameters (McKay et al. 2015, 2016). In order to use Equation (2), we corrected the effect by collisional quenching the O(^{1}D) atoms in the inner coma on the measured [O I] line intensity, according to McKay et al. (2015). We estimated the fraction of atoms lost to collisional quenching based on the Haser model including the quenching of O(^{1}D) atoms (Morgenthaler et al. 2001, 2007). Because we used a small aperture to extract the spectrum (the aperture size was 170 km × 2450 km at the observation), we assume that the H_2O molecules are the dominant source of O(^{1}D) (Raghuram & Bhardwaj 2013) and the dominant collision partner (Morgenthaler et al. 2001) in the inner coma. The water production rate of comet 21P/GZ at the observation was assumed to be $Q(H_2O) = 2.5 \times 10^{28}$ s^{-1} (Roth et al. 2020). Furthermore, not only the collisional quenching of O(^{1}D) but

Table 3
Photodissotiation Rates (at 1 au) and the Branching Ratio Used to Convert an Observed Green-to-red Line Ratio to a CO_2/H_2O Abundance Ratio

	Case (A)[a]	Case (B)[b]
$W_{H_2O}^{\rm green}$	3.20×10^{-8} s^{-1}	6.40×10^{-9} s^{-1}
$W_{H_2O}^{\rm red}$	8.00×10^{-7} s^{-1}	8.44×10^{-7} s^{-1}
$W_{CO_2}^{\rm green}$	7.20×10^{-7} s^{-1}	3.30×10^{-7} s^{-1}
$W_{CO_2}^{\rm red}$	5.25×10^{-7} s^{-1}	4.95×10^{-7} s^{-1}
$\beta^{\rm green}$	0.91[c]	0.91[c]

Notes.
[a] Raghuram & Bhardwaj (2013), converted to 1 au.
[b] McKay2015B in Table 6 of McKay et al. (2016).
[c] Slanger et al. (2006).

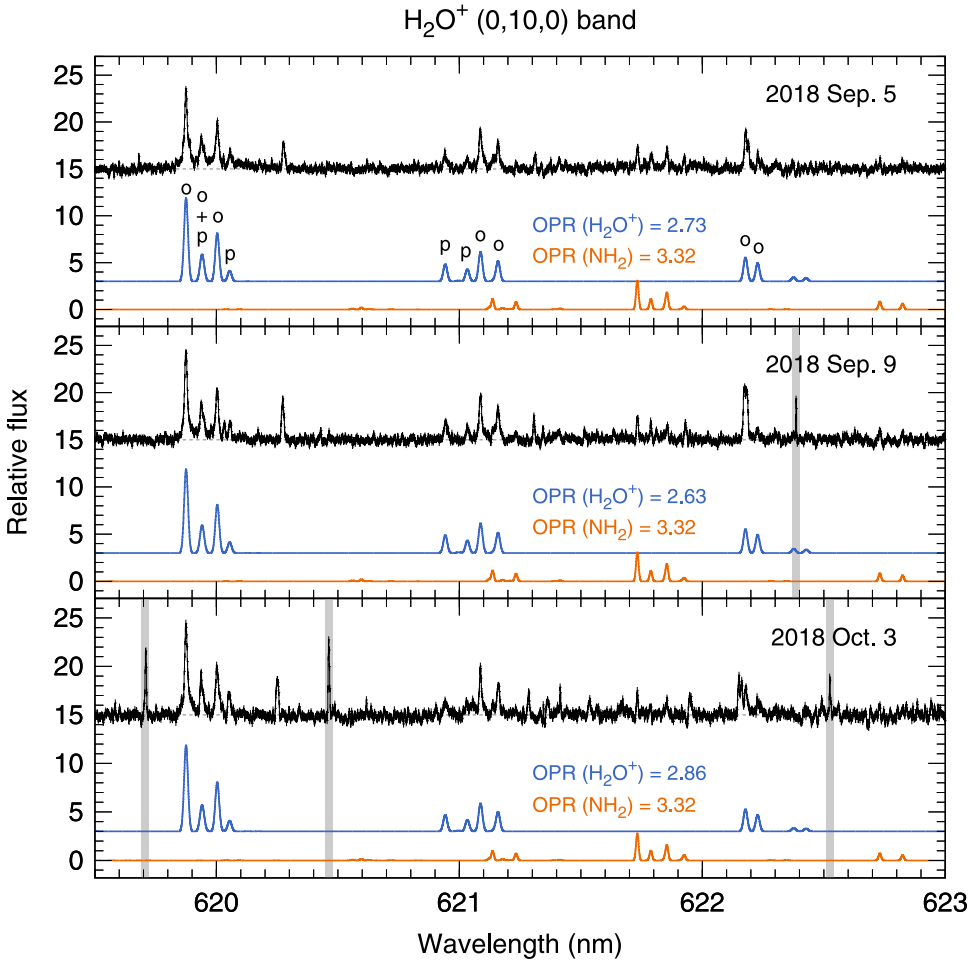

Figure 3. Comparison between the upper observed (in black, with an offset of 15) and lower modeled spectra of H_2O^+ (in blue, with an offset of 3) as well as NH_2 (in orange) with an OPR of 3.32 (the average value, see Table 4) on UT 2018 September 5, 9, and October 3. The ortho- and para-lines of H_2O^+ ("o" and "p," respectively) are labeled in the top panel. The vertical gray hatches indicate cosmic-ray artifacts.

Table 4
Summary of OPRs of NH_2 and H_2O^+ of 21P/GZ

UT Date	Sep 5	Sep 9	Oct 3	Average
NH_2				
$\nu_2 = 8$	3.07 ± 0.11	3.30 ± 0.09	3.26 ± 0.10	3.22 ± 0.06
$\nu_2 = 9$	3.34 ± 0.06	3.67 ± 0.08	3.14 ± 0.09	3.39 ± 0.05
$\nu_2 = 10$	3.20 ± 0.19	3.14 ± 0.14	3.34 ± 0.37	3.18 ± 0.11
Average	3.27 ± 0.05	3.45 ± 0.06	3.20 ± 0.07	3.32 ± 0.04
H_2O^+				
$\nu_2 = 10$	2.73 ± 0.30	2.64 ± 0.21	2.86 ± 0.18	2.76 ± 0.13

Note. ν_2 means (0, ν_2, 0) bands of NH_2 and H_2O^+.

also that of O(^{1}S) atoms are considered in our case. The rate coefficients for the collisional quenching of O(^{1}D) and O(^{1}S) by H_2O are the same as Decock et al. (2015). The scaling factor for the green-to-red line ratio is 0.58 in 21P/GZ on UT 2018 October 3. The derived CO_2/H_2O ratios for both parameter sets are listed in Table 2.

Figure 2 shows the CO_2/H_2O abundance in comets derived by different ways, in addition to our measurement (in case (A)). The values plotted in Figure 2 are derived from the [O I] green-to-red line ratios in consideration of the collisional quenching of the O(^{1}D) atoms (McKay et al. 2013, 2015, 2016), from the CO Cameron-band observations (Weaver et al. 1994), and from the direct measurements of H_2O and CO_2 by the Infrared Space Observatory (ISO) space observatory (Colangeli et al. 1999; Crovisier et al. 1999), the AKARI comet survey program (Ootsubo et al. 2012), the Spitzer space telescope (McKay et al. 2016), the Deep Impact spacecraft (A'Hearn et al. 2011; Gersch et al. 2018a, 2018b), and the Rosetta spacecraft (Bockelée-Morvan et al. 2016). Note that the CO_2/H_2O ratios derived from the [O I] green-to-red line ratios in Figure 2 are computed with the parameters of the case (A) in Table 3.

The comets in Figure 2 seem to be classified into two groups of comets whose CO_2/H_2O ratios are ∼10% and ∼25%, and the origin for the bimodal distribution is not clear. Although the CO_2/H_2O ratio might depend on the rotational phase of the cometary nucleus (A'Hearn et al. 2011), comet 21P/GZ is considered to be depleted in CO_2 compared to water, as shown in Figure 2. The line width of [O I] at 557.7 nm in comet 21P/GZ (∼2.1 km s^{-1}; Table 2) is at the lower end of the range of intrinsic line widths of [O I] at 557.7 nm in other comets (Cochran & Cochran 2001; Cochran 2008; Decock et al. 2013), and this fact is also suggestive of the low-CO_2 abundance in comet 21P/GZ because CO_2 might produce O(^{1}S) atoms with higher ejection velocities than H_2O. If we use the empirical parameters taken from McKay et al. (2015; case (B) in Table 3), the derived CO_2/H_2O ratio in comet 21P/GZ is 11.0 ± 0.3%, which is higher than that computed with the

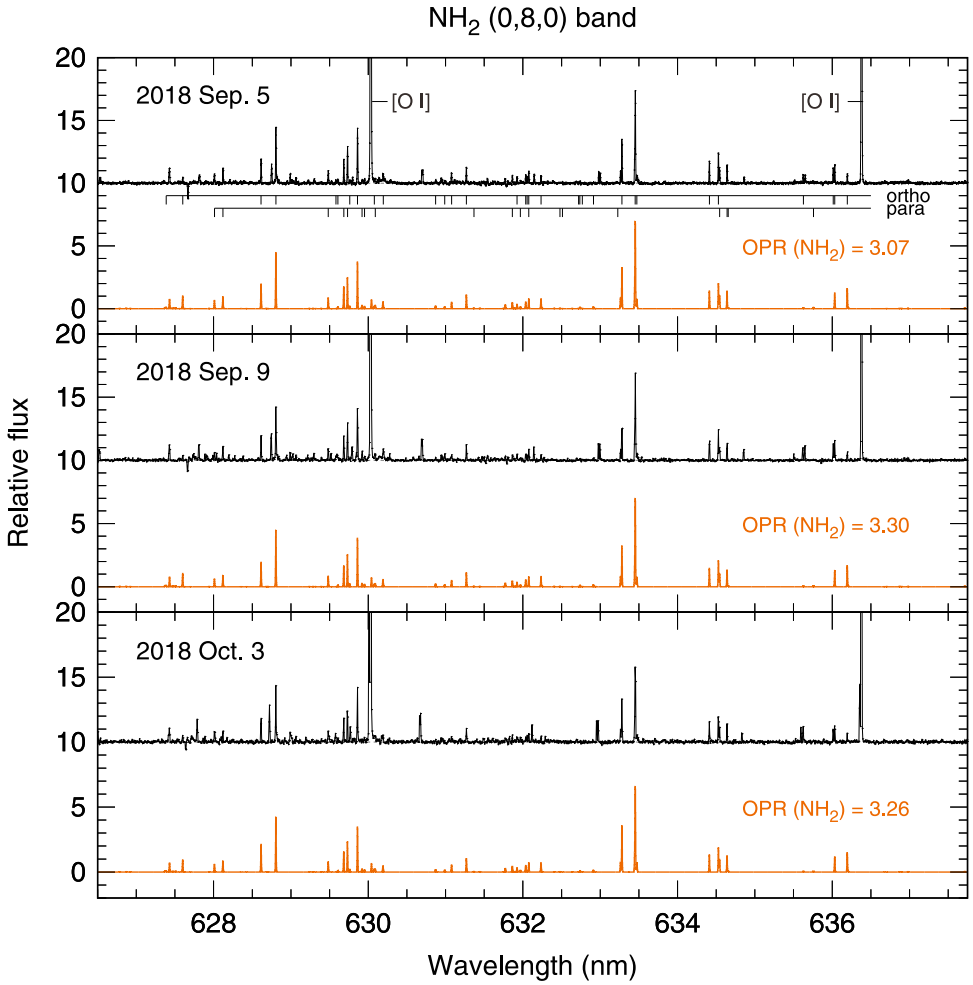

Figure 4. From top to bottom, comparison between the observed (in black, with an offset of 10) and modeled spectra of the NH_2 (0, 8, 0) band (in orange) on UT 2018 September 5, 9, and October 3. The ortho- and para-lines of NH_2 are labeled in these model spectra in the top panel. Two strong emission lines at 630.0 and 636.4 nm are identified as the [O I] lines labeled in the top panel.

parameters of the case (A) as shown above, but still in the low-CO_2 group (∼10%) in Figure 2. Such low-CO_2 abundance in comet 21P/GZ could be interpreted as the difference in comet-forming regions of these comets or some evolutional effects in the inner solar system for Jupiter-family comets. Ootsubo et al. (2019) recently proposed that comet 21P/GZ formed in a warmer region than other comets, based on their detection of complex organics in its low-resolution mid-infrared spectra. Our result, low-CO_2/H_2O in comet 21P/GZ, is consistent their hypothesis.

3.2. Abundance Ratio of the Nuclear Spin Isomer of the Water Cation (H_2O^+) and Amidogen (NH_2)

We measured the OPRs of water cations (H_2O^+) and amidogen (NH_2) in comet 21P/GZ from these rovibronic emissions in the high-resolution optical spectrum. Figure 3 plots the observed and modeled spectra of 21P/GZ around the H_2O^+ (0, 10, 0) band. The derived OPRs of H_2O^+ and NH_2 are listed in Table 4. Figure 3 shows that the derived OPR of H_2O^+ is 2.76 ± 0.13. Assuming the conservation of the total nuclear spin through the ionization reaction of water as the sole parent of H_2O^+, the OPR of H_2O^+ is the same as the OPR of water. Indeed, the OPR of water derived from the high-resolution near-infrared spectra of comet 21P/GZ in its 2005 and 2018 apparitions are OPR = 2.99 ± 0.23 (DiSanti et al. 2013) and 3.04 ± 0.12, respectively (Faggi et al. 2019). These values are consistent with the OPR of H_2O^+ obtained here within a 3σ error interval. The OPR of ammonia is also derived as 1.16 ± 0.02 based on the OPR of NH_2 in the comet (see Figures 4–6). Please note that the intensity ratio among bands is not correct because we scaled the intensity for each plot independently. The nuclear spin temperatures of water and ammonia are derived as $36 + 6/-3$ K from the OPR of H_2O^+ and 28 ± 1 K from the OPR of NH_2 even though the real meaning of the OPRs of water and ammonia are unclear.

Recent laboratory experiments demonstrate that the OPR of water is not the memory of its molecular formation (Hama et al. 2011, 2012, 2016, 2018; Hama & Watanabe 2013). It is likely that this is also for the case of ammonia (its OPR is estimated from NH_2). These laboratory results suggest that the OPRs of those molecules are initially the statistical weight ratios immediately following the sublimation from nucleus ice. The OPRs of cometary volatiles were probably modified by an ortho–para conversion process in the inner coma (or other catalyst activities of dust crust surfaces of the nucleus) rather than reflected by a temperature in the solar nebula, 4.6 Gyr ago,

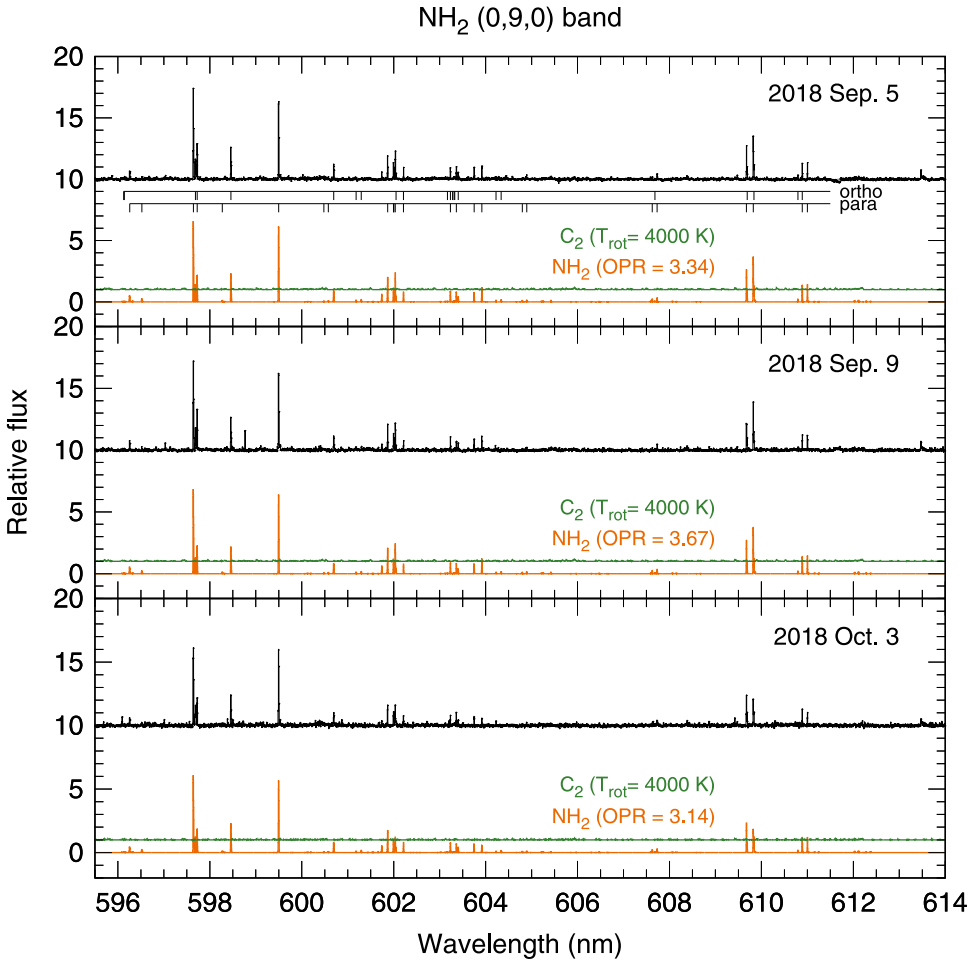

Figure 5. From top to bottom, comparison between the observed and modeled spectra of the NH_2 (0, 9, 0) band. The modeled spectrum of C_2 (in green, with an offset of 1) is also plotted on the NH_2 (0, 9, 0) band panels.

at the molecular formation. OPRs may be diagnostic for the physico-chemical conditions in the inner-most coma or beneath the surface.

3.3. Nitrogen Isotopic Ratio in NH_2

We also tried to measure the isotopic ratio of nitrogen in NH_2 ($^{14}N/^{15}N$) in comet 21P/GZ in the same manner as Shinnaka & Kawakita (2016). Despite clear observation of $^{14}NH_2$ (as shown in Figures 4 and 5), no emission lines of $^{15}NH_2$ could be detected compared with error levels. The lower limit of $^{14}N/^{15}N$ in 21P/GZ is >38 (3σ) and this value is consistent with the range obtained from previous measurements in cometary NH_2: 135.7 ± 5.9 (Shinnaka et al. 2016).

3.4. Formation Conditions of Comet 21P/Giacobini–Zinner

Finally, we discuss the origin of comet 21P/GZ. The depletion of simple organic molecules like C_2H_6, CH_3OH, and CO in this comet (DiSanti et al. 2013) is probably consistent with the depletion of carbon-chain molecules such as (C_2, C_3) and NH_2. However, these facts do not mean that the comet is depleted in more complex organics like polycyclic aromatic hydrocarbons (PAHs) and other hydrocarbons, as observed in 67P/Churyumov–Gerasimenko (Altwegg et al. 2019). The observed property of linear polarization produced by cometary dust grains indicates the possible existence of complex organic matter (Kiselev et al. 2000). Furthermore, Ootsubo et al. (2019) recently reported the detection of unidentified infrared emission features attributed to complex organic molecules such as PAHs in comet 21P/GZ. Because more complex molecules could form under warmer conditions, comet 21P/GZ might have formed in a warmer region than where other comets formed in the solar nebula. Depletion in highly volatile molecules such as C_2H_6, CH_3OH, and CO supports this hypothesis. The CO_2/H_2O ratio in 21P/GZ obtained from our observation is also depleted and consistent with the formation under warmer conditions. The fluffy and fragile grains of meteoroids of the October Draconids meteor shower are also indicative of dust aggregation by organic materials acting as glue.

If comet 21P/GZ formed in the inner region of the solar nebula, the dust grains of the comet may contain more abundant crystalline silicates (formed in the inner-most coma and transported to the comet-forming region) compared to other comets. However, the crystalline-to-amorphous ratio in silicate grains in comet 21P/GZ is typical among comets (Ootsubo et al. 2019). Therefore, Ootsubo et al. (2019) proposed the hypothesis that comet 21P/GZ formed in the circum-planetary disk of giant planets where is warmer than the surrounding solar nebula.

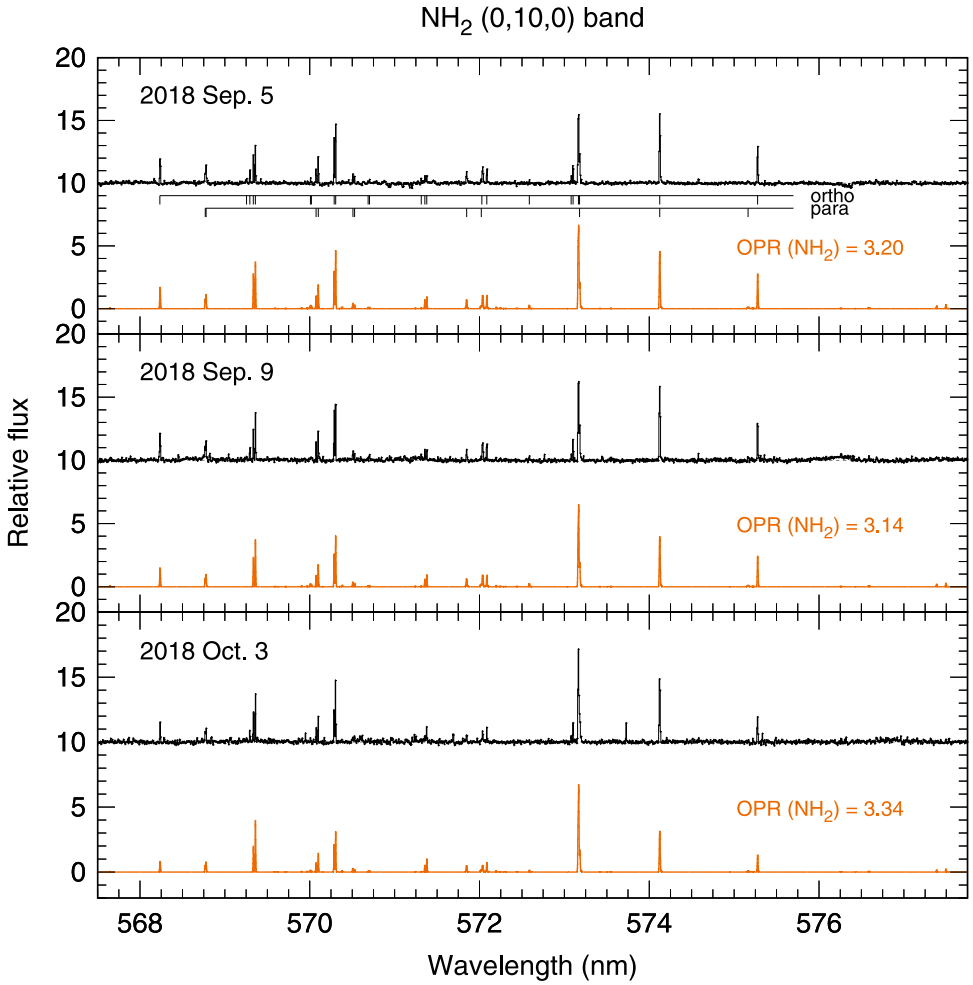

Figure 6. From top to bottom, comparison between the observed and modeled spectra of the NH_2 (0, 10, 0) band. In the NH_2 (0, 10, 0) band panels, it appears that the model cannot reproduce certain strong lines because of the significant line splitting by perturbations described in Shinnaka et al. (2010). The lines affected by the perturbations were simply summed over, and the result was compared with the calculation for each unperturbed line.

This paper is based on data collected at the Subaru Telescope, which is operated by the National Astronomical Observatory of Japan. We would like to thank Editage (www.editage.com) for English language editing.

Software: IRAF (Tody 1986, 1993), LBLRTM code (Clough et al. 1992).

ORCID iDs

Yoshiharu Shinnaka https://orcid.org/0000-0003-4490-9307
Hideyo Kawakita https://orcid.org/0000-0003-2011-9159
Akito Tajitsu https://orcid.org/0000-0001-8813-9338

References

A'Hearn, M. F., Belton, M. J. S., Delamere, W. A., et al. 2011, Sci, 332, 1396
Altwegg, K., Balsiger, H., & Fuselier, F. A. 2019, ARA&A, 57, 113
Bhardwaj, A., & Raghuram, S. 2012, ApJ, 748, 13
Bockelée-Morvan, D., Crovisier, J., Erand, S., et al. 2016, MNRAS, 462, S170
Borovička, J., Kooten, P., Shrbený, L., et al. 2010, in IAU Symp. 263, Icy Bodies of the Solar System, ed. J. A. Fernandez et al., 218
Borovička, J., Kooten, P., Shrbený, L., Rostislav, Š, & Hornoch, K. 2014, EM&P, 113, 15
Capria, M. T., Gremonese, G., & de Sanctis, M. C. 2010, A&A, 522, A82
Cessateur, G., de Keyser, J., Maggiolo, R., et al. 2016, JGR, 121, 804
Clough, S. A., Iacono, M. J., & Moncet, J.-L. 1992, JGR, 97, 15761
Cochran, A. L. 2008, Icar, 198, 181
Cochran, A. L., & Cochran, W. D. 2001, Icar, 154, 381
Colangeli, L., Epifani, E., Brucato, J. R., et al. 1999, A&A, 343, L87
Crovisier, J., Encrenaz, Th., Lellouch, E., et al. 1999, in The Universe as Seen by ISO, ed. P. Cox & M. F. Kessler (Noordwijk: ESA), 161
Decock, A., Jehin, E., Hutsemékers, D., & Manfroid, J. 2013, A&A, 555, A34
Decock, A., Jehin, E., Rousselot, P., et al. 2015, A&A, 573, A1
Dello Russo, N., Kawakita, H., Vervack, R. J., Jr., & Weaver, H. A. 2016, Icar, 278, 301
DiSanti, M. A., Bonev, B. P., Villanueva, G. L., & Mumma, M. J. 2013, ApJ, 763, 1
Faggi, S., Mumma, M. J., Villanueva, G. L., Paganini, L., & Lippi, M. 2019, AJ, 158, 254
Fink, U. 2009, Icar, 201, 311
Galavis, M. E., Mendoza, C., & Zeippen, C. J. 1997, A&AS, 123, 159
Gersch, A. M., Feaga, L. M., & A'Hearn, M. F. 2018a, ApJ, 854, 149
Gersch, A. M., Feaga, L. M., & A'Hearn, M. F. 2018b, ApJ, 856, 104
Hama, T., Kouchi, A., & Watanabe, N. 2016, Sci, 351, 65
Hama, T., Kouchi, A., & Watanabe, N. 2018, ApJL, 857, L13
Hama, T., Kuwabata, K., Watanabe, N., et al. 2012, ApJ, 757, 185
Hama, T., & Watanabe, N. 2013, ChRv, 113, 8783
Hama, T., Watanabe, N., Kimura, Y., et al. 2011, ApJ, 738, 15
Huestis, D., & Slanger, T. G. 2006, BAAS, 38, 609
Jenniskens, P. 2006, Meteor Showers and their Parent Comets (Cambridge: Cambridge Univ. Press)
Kawakita, H., Ayani, K., & Kawabata, T. 2000, PASJ, 52, 925
Kiselev, N. N., Jockers, K., Rosenbush, V. K., et al. 2000, P&SS, 48, 1005
Kurucz, R. L. 2005, MSAIS, 8, 189

McKay, A. J., Chanover, N. J., Jeffrey, P., et al. 2013, Icar, 222, 684
McKay, A. J., Cochran, A. L., DiSanti, M. A., et al. 2015, Icar, 250, 504
McKay, A. J., Kelley, M. S. P., Cochran, A. L., et al. 2016, Icar, 266, 249
Morgenthaler, J., Harris, W. N., & Cimbi, M. R. 2007, ApJ, 657, 1162
Morgenthaler, J., Harris, W. N., Scherb, F., et al. 2001, ApJ, 563, 451
Noguchi, K., Aoki, W., Kawanomoto, S., et al. 2002, PASJ, 54, 855
Ootsubo, T., Kawakita, H., Hamada, S., et al. 2012, ApJ, 752, 15
Ootsubo, T., Kawakita, H., Shinnaka, Y., Watanabe, J., & Honda, M. 2019, Icar, 338, 113450
Raghuram, S., & Bhardwaj, A. 2013, Icar, 223, 91
Roth, N. X., Gibb, E. L., Bonev, B. P., et al. 2020, AJ, 159, 42
Rousselot, P., Decock, A., Korsun, P. P., et al. 2015, A&A, 580, A3
Rousselot, P., Jehin, E., Manfroid, J., & Hutsemékers, D. 2012, A&A, 545, A24
Rubin, M., Altwegg, K., van Dishoeck, E. F., & Schwehm, G. 2015, ApJL, 815, L11
Shinnaka, Y., & Kawakita, H. 2016, AJ, 152, 145
Shinnaka, Y., Kawakita, H., Kobayashi, H., & Kanda, Y. 2010, PASJ, 62, 263
Shinnaka, Y., Kawaktia, H., Jehin, E., et al. 2016, MNRAS, 462, S195
Slanger, T. G., Cosby, P. C., Sharpee, B. D., Minschwaner, K. R., & Siskind, D. E. 2006, JGR, 111, A12318
Song, Y., Gao, H., Chang, Y. C., et al. 2014, PCCP, 16, 563
Storey, P. J., & Zeippen, C. J. 2000, MNRAS, 312, 813
Tody, D. 1986, Proc. SPIE, 627, 733
Tody, D. 1993, in ASP Conf. Ser. 52, Astronomical Data Analysis Software and Systems II, ed. R. J. Hanisch, R. J. V. Brissenden, & J. Barnes (San Francisco, CA: ASP), 173
Weaver, H. A., Feldman, P. D., McPhate, J. B., et al. 1994, ApJ, 422, 374